



Contents lists available at ScienceDirect

Sensors and Actuators: B. Chemical

journal homepage: www.elsevier.com/locate/snb

Reduced graphene quantum dot based versatile platform for L-dopa sensing: Fluorescence turn-on, filter paper, and air-stable flexible electronic devices

Kangkan Jyoti Goswami^{a,b}, Bedanta Gogoi^{c,*}, Neelotpal Sen Sarma^{a,b,**}

^a Advanced Materials Laboratory, Institute of Advanced Study in Science and Technology, Paschim Borigaon, Guwahati 35, Assam, India

^b Academy of Scientific and Innovative Research (AcSIR), Ghaziabad 201002, India

^c Department of Chemistry, Gauhati University, Jalukbari, Guwahati 14, Assam, India

ARTICLE INFO

Keywords:

Reduced graphene quantum dot
Fluorescence turn-on
Aggregation-induced-emission, current-voltage characteristics
L-dopa

ABSTRACT

L-dopa is a chiral drug that has been extensively used for the treatment of Parkinson's disease. The concentration of L-dopa plays a vital role in the treatment, and this work emphasizes on designing a versatile platform for the quantitative and selective detection of L-dopa using reduced graphene quantum dot (rGQD). The platform is efficient in three different sensing methods, viz. fluorescence turn-on, filter paper-based sensing, and electronic measurements. The rGQD undergoes a dramatic fluorescence turn-on in the presence of L-dopa in aqueous media and artificial urine with a detection limit as low as 1.307 μM and 1.217 μM respectively. Experimental evidence revealed that the fluorescence enhancement is attributed to aggregation-induced emission mechanism. The system is also applicable for visual detection of L-dopa using filter paper strips treated with rGQD and develops bright fluorescence under ultra-violet irradiation. Apart from this, electrical sensors for L-dopa were also developed by preparing rGQD treated poly-vinyl alcohol films, and the increase in the current conduction with varying concentrations of L-dopa was observed. The films produce 2.5 order higher current conduction at 300 μM of L-dopa with a detection limit of about 13.136 μM . At the final stage, we have designed flexible electronic devices using these materials that develop 1.3 order higher current for L-dopa. The devices exhibit excellent air stability under varied relative humidity conditions as well as high bending stability for potential practical applications.

1. Introduction

Parkinson's disease, named after the physician Dr. James Parkinson [1], is a neurodegenerative disorder [2] that affects movements of the body [3]. It is associated with several motor symptoms like rigidity, micrographia, tremor at rest, postural instability, and shuffling gait [4, 5]. A severe shortage of neurotransmitters dopamine in substantia nigra and the presence of Lewy bodies is the primary cause of Parkinson's disease [6]. Tremendous progress has been made to evaluate the neurophysiological mechanism involved in the disease progression; above all, the most efficacious therapy based on L-dopa treatment [7], considered as Gold standard [8] for Parkinson disease. 1-3,4-dihydroxyphenylalanine, commonly known as L-dopa, is a prominent chiral drug used in the treatment of Neurodegenerative Parkinson's disease (PD) caused by a severe shortage of neurotransmitters dopamine in substantia

nigra pars compacta [9]. In the presence of dopacarbonylase enzyme in the brain, L-dopa is converted to dopamine and stored in dopaminergic neurons. In contrast, dopamine itself can't penetrate the blood-brain barrier [10]. As the disease progresses, with continuous loss of neurons, the clinical benefit from each dose of L-dopa progressively shortens [11]. Consequently, deterioration in their symptoms such as Parkinsonism, anxiety, and depression or higher concentrations that result in dyskinesias, psychosis, and orthostatic hypotension appears [12,13]. Therefore, to maintain the therapeutic effectiveness, the concentration of L-dopa must be adjusted to avoid adverse effects [14]. The Development of efficient L-dopa sensors will be beneficial in this regard, and hence we developed a new and versatile method for the selective detection of L-dopa via fluorescence turn-on measurements, filter paper-based observation, and flexible electronic devices for electrical measurements using reduced graphene quantum dot (rGQD) as the

* Corresponding author.

** Corresponding author at: Advanced Materials Laboratory, Institute of Advanced Study in Science and Technology, Paschim Borigaon, Guwahati 35, Assam, India.

E-mail addresses: bedanta@gauhati.ac.in (B. Gogoi), neelot@iasst.gov.in (N.S. Sarma).

<https://doi.org/10.1016/j.snb.2021.130892>

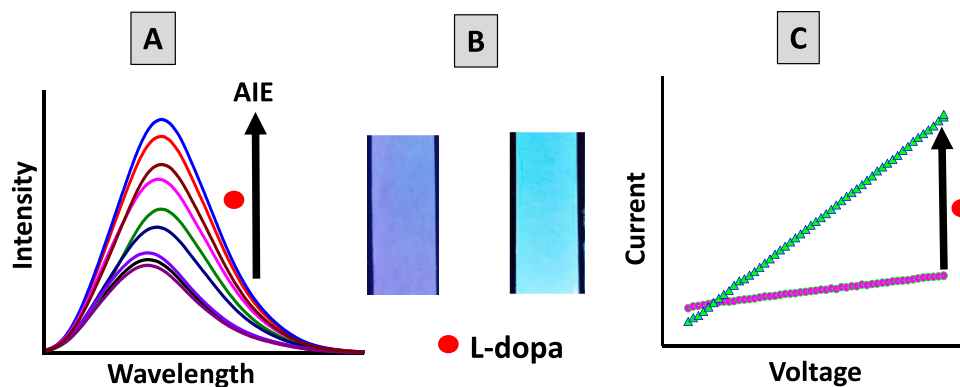
Received 16 July 2021; Received in revised form 11 September 2021; Accepted 7 October 2021

Available online 9 October 2021

0925-4005/© 2021 Elsevier B.V. All rights reserved.

sensing material. Graphene-based quantum dots possess unique optical and physicochemical properties mainly, large surface-to-volume ratio, excellent thermal and electrical conductivity, biocompatibility, and has received considerable attention as a potential candidate for biosensor application [15,16]. Over the past few decades, developing biosensors based on graphene-based materials has great attention for disease management and health care monitoring because of its high sensitivity, portability, rapid, low-cost operation, and ease of use [17]. Wearable biosensors have additional benefits of real-time application, convenient operation, quick response, portability, and inherent miniaturization [18] towards the diagnostics of disease [19].

In literature, there are a few reports available for the selective detection of L-dopa based on fluorescence turn-off/on mechanism [20–23]. Other common techniques used for the sensing are colorimetric [24], electrochemical methods [10,13], high-performance liquid chromatography [25], and spectrophotometry methods [26]. Among all these techniques, fluorescence turn-on sensors are more attractive and efficient among fluorescence-based sensing due to their high selectivity, sensitivity, and higher resolution ability [20]. One of the main reasons for fluorescence turn-on is aggregation-induced emission (AIE). AIE is a special case in the fluorescence process and was first observed by Tang et al. in silole molecules in the year 2001 [27]. Since then, many efforts have been made by both theoretical and experimental researchers to establish the underlying mechanism of AIE as well as exploring its high technological applications in various domains. As reported earlier, the most commonly accepted cause for the AIE is the restriction of intramolecular motions (RIM) such as rotational and vibrational motions. Due to these restrictions, the radiative decay process or fluorescence becomes predominant over the nonradiative decay. This was experimentally validated by incorporating chromophores, lowering the temperature, and doping in a rigid polymer matrix and metal-organic frameworks [28–30]. Various factors such as structural rigidity, the viscosity of the medium, temperature, doping of chromophores in rigid matrices can cause strong emission [31]. In recent years, AIE was also observed in carbon quantum dots [32,33] and GQDs [34,35]. In the current context, AIE was observed during the fluorescence sensing of L-dopa in aqueous media. This fluorescence enhancement was also found to be helpful in designing filter paper-based fluorescence turn-on sensor for L-dopa. Such paper-based sensing processes are very simple, inexpensive, and convenient to use [36]. On the other hand, interaction with the analyte significantly alters the electrical properties of the sensor system making it suitable for designing flexible devices. To the best of our knowledge, filter paper-based, and flexible electronic device-based L-dopa sensors have not been reported earlier. We believe that these findings will open up research in a new direction in this area which will help develop low-cost and efficient technologies for such bio-medical applications. The three major observations made in this work are shown in Scheme 1.



Scheme 1. Pictorial representation for the triple mode sensing of L-dopa, A. Aggregation induced emission (AIE) based fluorescence turn-on, B. Filter paper-based sensor, C. Current-voltage measurements.

2. Experimental section

2.1. Material development

2.1.1. Materials used

Graphite flakes, sodium hydroxide (NaOH), sulfuric acid (H₂SO₄), potassium permanganate (KMnO₄), sodium nitrate (NaNO₃), Poly-vinyl alcohol (PVA), blood plasma was obtained from Sigma-Aldrich. Ethylenediamine (EDA) was obtained from SRL. All the chemicals were used without any further purification. Milli-Q water was used for all the reactions.

2.1.2. Preparation of graphene oxide (GO)

GO was synthesized from graphite using the modified Hummer's method [37]. In brief, 0.5 g of NaNO₃ and 0.5 g of graphite flakes were mixed with 23 mL of 12.1 M H₂SO₄ (98%) and stirred for 15 min at 0–3 °C. In this mixture, 4 g of KMnO₄ was slowly added by keeping the temperature below 20 °C. The reaction mixture was then stirred for 90 min, maintaining the temperature of 40 °C, followed by dilution with 50 mL double distilled water under vigorous stirring for 10 min. The dark brown suspension of this mixture was treated with 6 mL 30% H₂O₂ solution and dilute with 50 mL double distilled water. The excess manganese salt was removed by washing several times with deionized water until pH becomes 7. Finally, the purified GO was dried and stored in desiccators over CaCl₂ for further experiment.

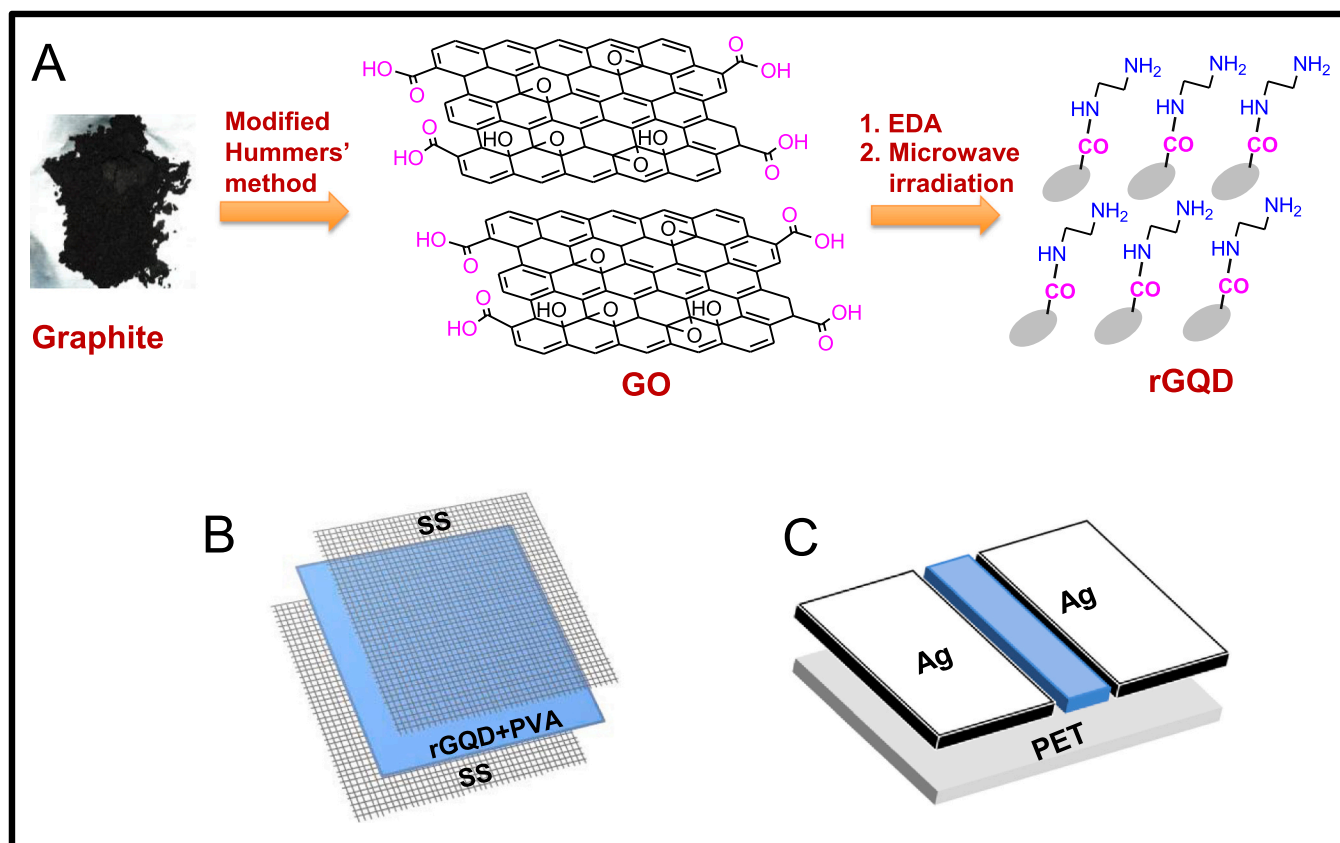
2.1.3. Preparation of reduced graphene quantum dots (rGQD)

rGQD was prepared using microwave-assisted pyrolysis methods to prepare rGQD. Firstly, 100 mg of graphene oxide (GO) was mixed in deionized water (1 mg/mL) followed by exfoliation using ultrasonication for 3 h. To this, EDA was added under vigorous stirring at room temperature. The reaction mixture was heated using microwave irradiation for 10 min at 500 Watt power. The resultant solution was centrifuged under 10,000 rpm, and the upper portion of the solution containing rGQD was stored for further use. Preparation of GO and rGQD from graphite is shown in Scheme 2A.

2.2. Sensing experiments

2.2.1. Fluorescence-based sensing

Aqueous solutions of L-dopa was prepared at a concentration ranging from 3 μM to 300 μM. Freshly prepared L-dopa solution of a particular concentration was mixed thoroughly with 2 mL of prepared rGQD solutions in a quartz cuvette using excitation wavelength (λ_{ex}) at 350 nm. The same procedure has been applied for detecting L-dopa spiked in artificial urine (AU) to investigate the applicability of the method in the real sample.



Scheme 2. Pictorial representation for the A. Synthesis of rGQD from graphite, B. rGQD + PVA (8% W/V) film for electrical measurements, C. Flexible device for sensing experiments.

2.2.2. Filter paper-based sensing

Firstly, Whatman filter paper (grade-1) was cut into small pieces of 1 cm × 5 cm strips and treated with rGQD solution for five minutes. After that, these rGQD coated filter paper strips were dried in a hot air oven for 20 min. For visual detection of L-dopa, the prepared filter paper strips were treated with varying L-dopa concentrations in distilled water, and their digital photographs were taken under an ultraviolet (UV) cabinet with 365 nm UV monochromatic light. The same protocol has been followed for the L-dopa samples prepared in AU to mimic the real-sample analysis.

2.2.3. Electrical measurements based sensing

For electrical measurements, oven-dried rGQD + PVA (8% W/V) films were cut into pieces with 1 cm² area and sandwiched in between stainless steel (SS) mesh with 200 μm pore size (Scheme 2B). After that, these films were treated with different L-dopa concentrations (10–300 μM) and dried in a vacuum desiccator. The change in the current-voltage (*I*-*V*) characteristics and the impedance (*Z*) of the rGQD + PVA (8% W/V) films were monitored using an impedance analyzer (HIOKI 3532-50) and electrometer (Keithley 6517B) at room temperature.

2.2.4. Flexible devices fabrication

To fabricate air-stable and flexible devices, we have blended rGQD with 8% PVA W/V by magnetic stirring and deposited it on poly(ethylene terephthalate) (PET) substrates, followed by oven drying at 60 °C for 4 h. After that, silver paste was deposited with 0.5 × 1 cm² area with a separation of 2 mm (Scheme 2C). All the devices were kept in a vacuum desiccator for further use. The idea behind using 8% PVA W/V is to provide a stretchable platform required for performing the experiments at different bending angles. This also ensures better contact

with the substrate and the electrodes.

2.3. Characterization techniques

The Fourier transform infrared (FT-IR) studies were carried out in PerkinElmer FT-IR spectrophotometer by mixing the sample with KBr pellet; the measurements were performed in transmission mode over 32 scans. X-ray diffraction (XRD) patterns were recorded using a Bruker D8 Advance X-ray diffractometer with Cu K α radiation, at a scan rate of 2 s per step. The tube current and voltage were maintained at 40 mA and 40 kV, respectively, with 2 θ = 10–90° angular range. Electronic transitions were monitored by UV-Vis spectra at room temperature using a 1800 SHIMADZU UV-Vis spectrophotometer. The fluorescence spectra were collected using a Cary Eclipse spectrophotometer with a constant scan rate of 240 nm/s with a halogen lamp as the excitation source. The excitation and emission slit widths were maintained at 5 nm with an applied voltage 700 V. All fluorescent spectacle measurements were carried out using Quartz cells (4 × 1 × 1 cm) with high vacuum Teflon stopcocks. The fluorescence lifetime of the samples in aqueous media was determined using Edinburgh instruments FSP920, Picosecond Time-resolved cum Steady State Luminescence Spectrometer. An LED source of wavelength 350 nm was used as the excitation source. Zeta potential and hydrodynamic diameter of the particles were measured in Malvern NanoZS90 in a glass cuvette with a square aperture with zeta dip cell electrode at room temperature. Transmission electron microscope (TEM) data were studied on the JEOL TEM-2100 model by drop-casting the rGQD on a 3 mm copper grid covered with carbon film and kept in a desiccator. The surface morphology of the rGQD + PVA films were studied with a SIGMA VP (ZEISS) FESEM at an accelerating voltage of 5 kV. The electrical measurements were performed using HIOKI 3532-50, LCR Hi-TESTER.

3. Results and discussions

3.1. Materials characterization

The rGQD so prepared is well characterized with the help of UV–vis, photoluminescence, and FT-IR spectroscopic analysis, XRD, and TEM analysis, as discussed below.

Supplementary Material Fig. S1A shows the UV–visible absorption spectra of GO and rGQDs. Here, GO exhibits a characteristic absorption peak at 227 nm, presumably due to the $\pi \rightarrow \pi^*$ transition of C=C bond, along with a shoulder peak appears at 302 nm corresponding to the $n \rightarrow \pi^*$ transition of C=O bonds [38]. The reduction of GO by EDA in water is confirmed by the red-shift of the peak at 227–317 nm, which is probably due to the restoration of delocalized double bond along with high polarity solvent media [39].

Fig. S1B represents the typical fluorescence spectra of rGQD recorded in aqueous media with varying excitation wavelengths from 300 nm to 550 nm. It is evident that the emission spectra position undergoes red-shift and the intensity gradually decreases with the increase in the excitation wavelength.

The FT-IR spectra of pure GO (Fig. S1C) exhibit characteristic absorption bands at 1061 cm^{-1} , 1222 cm^{-1} , and 1397 cm^{-1} corresponding to C-O stretching vibration in alkoxy group, epoxy group, and carboxylic group respectively. The appearance of the strong stretching bands at 1632 cm^{-1} , 1723 cm^{-1} and 3433 cm^{-1} correspond to the functional groups C=C (in the aromatic ring), C=O (in carboxylic acid), and O-H group, respectively [40]. Reduction of GO with EDA is confirmed by the disappearance of the peak at 1723 cm^{-1} corresponding to the C=O stretching vibration of carboxylic acid and the appearance of a new peak at 1635 cm^{-1} and 1579 cm^{-1} corresponding to C=O and N-H stretching vibration for secondary amide group, respectively [41]. Amide fictionalization is further confirmed due to the appearance of the peaks at 1327 cm^{-1} and 1158 cm^{-1} corresponds to C-N stretching vibrations [42]. When out-of-plan NH_2 and NH couple with C-N antisymmetric

stretching vibration, a weak intensity peak at 1486 cm^{-1} was observed in rGQD interferogram [43].

To further confirm the formation of GO and rGQD, the XRD patterns were observed, as shown in Fig. S1D. Neutral graphite shows a basal reflection (002) diffraction peak at $2\theta = 26.6^\circ$ [41]. However, shifting of 002 reflection peak at $2\theta = 10.85$, corresponding to a d spacing of 0.81 nm reveals the interaction of oxygen-containing functionalities between the basal plane of graphene [39]. The XRD pattern of rGQDs shows a broad peak at $2\theta = 24.11$, inferred that the layered structure of graphene oxide is exfoliated to a few layers by simultaneous reduction and surface modification by EDA.

3.2. Sensing experiments

3.2.1. Fluorescence-based sensing

The main advantage of fluorescence-based sensing using our material is that it showed a dramatic increase in the fluorescence intensity of rGQD in the presence of an increasing concentration of L-dopa in aqueous media, as shown in Fig. 1A. Also, the intensity of the emission is proportional to the concentration of L-dopa. This increase in the fluorescence intensity is significantly higher than the earlier reports [11,23]. The difference in the fluorescence intensity ($F-F_0$) was plotted after the addition of L-dopa for a definite time interval as shown in the supplementary material Fig. S2. The plots reach a saturation point at 4 min (Fig. S2). Additionally, it is useful for visual detection and hence practically more favorable over the turn-off processes. To demonstrate the practical applicability of the proposed biosensor, the real-sample analysis was carried out in AU samples by spiking different quantities of L-dopa ranging from 5 to 300 μM with AU Fig. 1B. From the calibration plots (Fig. 1C and D), the limit of detection (LOD) was calculated using the equation $\text{LOD} = 3.3 \times \text{RSD}/\text{Slope}$ and found to be 1.307 μM and 1.217 μM for aqueous and AU, respectively. Here, RSD stands for relative standard deviation. This indicates that the rGQD is a potential candidate for sensing L-dopa not only in aqueous samples but also in real

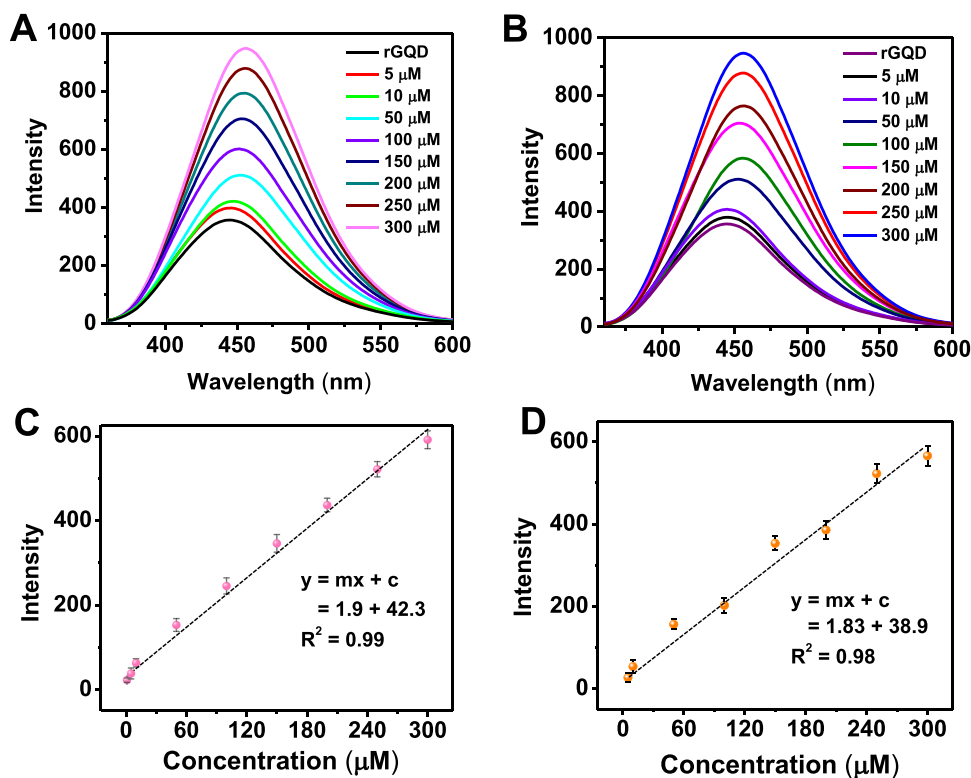


Fig. 1. PL spectra of A. rGQD + L-dopa in aqueous media, B. rGQD + L-dopa in artificial urine. Calibration plot of C. rGQD + L-dopa in aqueous media, D. rGQD + L-dopa in artificial urine.

samples.

In the UV–vis spectral analysis, as shown in Fig. S3A, the absorption of the pure L-dopa was observed at around 279 nm, which undergo red-shift to 295 nm indicating the aggregation of the analyte and the sensor. Considering the chemical architectures, the occurrence of red-shift is presumed to be due to the formation of hydrogen bonding or electrostatic interaction between the sensing material and the analytes, as shown in Fig. S3B [44]. This has been confirmed with the help of TEM analysis, ‘salt-screening effect’, and DLS measurements as discussed later. To further investigate the selectivity of the method, we checked the fluorescence response of the rGQD in the presence of various ions, amino acids, urea, uric acid, and ascorbic acid, as shown in Fig. 2A, and there was no such fluorescence turn-on for all these analytes.

3.2.2. Effect of pH towards fluorescence enhancement

To evaluate the optimal conditions for fluorescence turn-on detection of L-dopa, the fluorescence intensities of rGQD as well as in the presence of 50 μM L-dopa in PBS buffer solution at different pH ranging from 1.0 to 11 were recorded as shown in Fig. 2B. The relative fluorescence intensity value, $\Delta F = (F-F_0)$ increased with increasing pH from 1 to 7 along with the blue-shift in the emission spectrum. It was observed that the maximum PL intensity was attained at $\text{pH} = 7$ and reduced when pH increases from 7 to 11. The observed changes in spectral properties can be useful to evaluate the optimal condition towards the fluorescence response of the rGQD sensor at different pH levels.

3.2.3. Mechanism of sensing

To find out the reason behind the fluorescence turn-on in our system, we checked the TEM images of the mixture solution right after the sensing experiment. The rGQD particles are spherical, and the average particle size was found to be about 4 nm (Fig. 3A). But, after the interaction with L-dopa, aggregated and large particles were observed in the TEM images, as evident from Fig. 3B, which indicates the occurrence of aggregation-induced emission (AIE) in the fluorescence measurements. In literature, it was found that in addition to the enhancement of fluorescence intensity, the occurrence of AIE also increases the fluorescence lifetime [45]. In the present context, the initial fluorescence lifetime was calculated to be 2.12 ns, which increases to 2.8 ns after the interaction with L-dopa. This observation confirms the occurrence of AIE in the sensor-analyte system. The fluorescence decay profiles are shown in Fig. S4.

The presence of electrostatic interactions between rGQD and L-dopa is the driving force for such aggregation and confirmed by performing the well-known experiment called the ‘salt-screening effect’. Here, the presence of a highly ionized salt in the aqueous solution prevents the electrostatic interaction among the other components. We have performed the sensing experiment in the presence of a higher concentration

of KCl solution (2 M) and observed that in the presence of KCl, the intensity of the mixture solution doesn't further increase with the increasing concentration of L-dopa (Fig. 3C) [46]. Another way to study the existence of electrostatic interaction is to determine the change in the zeta-potential values of the system before and after the sensing experiment. A detailed study is given in the later section. On the other hand, a comparative spectroscopic analysis of the chemical composition of the material before and after the sensing experiment can provide information related to the presence or absence of permanent chemical interaction between the sensor and the analyte [46,47]. Here, we have performed the FT-IR spectral analysis and found that the intensity of the initial peak position of the rGQD at 1635 cm^{-1} significantly diminished after the interaction with L-dopa. Again, the peak at 1579 cm^{-1} shifted to 1562 cm^{-1} . From these observations, it has been confirmed that both the C=O and N-H groups present in rGQD takes part in hydrogen bonding with the analyte as shown in Fig. S3B [46].

Fig. 4 depicts the particle size distribution of the sample in aqueous media before and after the interaction with the analyte. It was found that the initial particle size of the rGQD was about 6 nm (Fig. 4A), but after the interaction with L-dopa, the value significantly increased to about 73 nm (Fig. 4B). Therefore, there was a twelve-fold increase in the hydrodynamic diameter of the system which is in agreement with the TEM analysis as discussed earlier (Fig. 3A and B). Therefore, both the TEM and DLS studies have provided conclusive evidence of aggregation in the system. Corresponding zeta-potential values are shown in Fig. 5. Here, L-dopa and rGQD both possess a negative zeta-potential value of about -17.0 mV and -43.0 mV respectively (Fig. 5A and B). After the interaction with L-dopa, the zeta-potential decreases to about -33.0 mV (Fig. 5C). Such a notable difference in the zeta-potential value provides strong evidence of the electrostatic interaction associated with the system. Decrease in the zeta-potential value facilitates particle aggregation that leads to AIE in the fluorescence process [48]. Previous reports emphasized the change in the zeta-potential of the sensing platforms governed by electrostatic interactions [49–51]. The results of the DLS measurements thus comply with previously reported work where AIE was the main reason for the fluorescence turn-on [46].

3.2.4. Practical applicability of the method

In literature, it was found that the expected value of L-dopa in plasma of a patient is $3.5\text{ }\mu\text{g mL}^{-1}$ [52]. To demonstrate the practical applicability of the proposed biosensor, real sample analyses were carried out in commercially available human blood plasma. The simultaneous determination of L-dopa in blood plasma by spiking different quantities of analyte ranging from $5\text{ }\mu\text{M}$ to $300\text{ }\mu\text{M}$ were performed through calibration curve methods. Three consecutive measurements ($n = 3$) have been performed to determine the RSD. The accuracy of this method was evaluated by determining the recovery of the spike which was found to

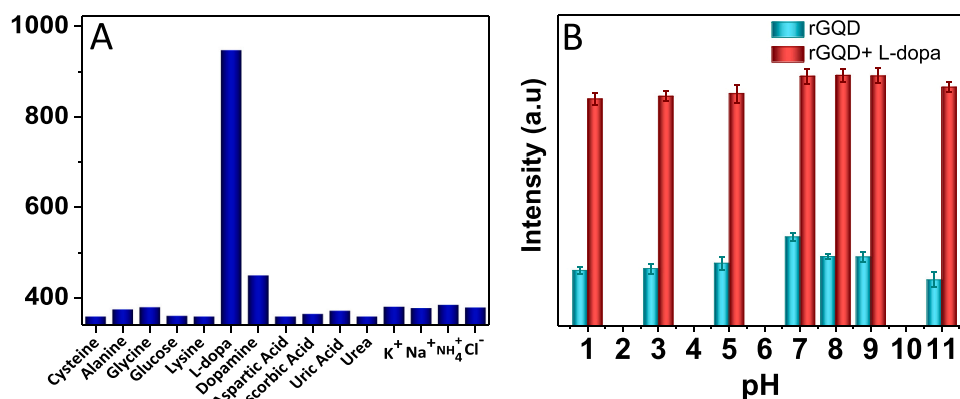


Fig. 2. A. Histogram of the fluorescence intensity of rGQD in the presence of various ions, amino acids, bio-chemicals. B. Histogram of the fluorescence intensity of rGQD at different pH.

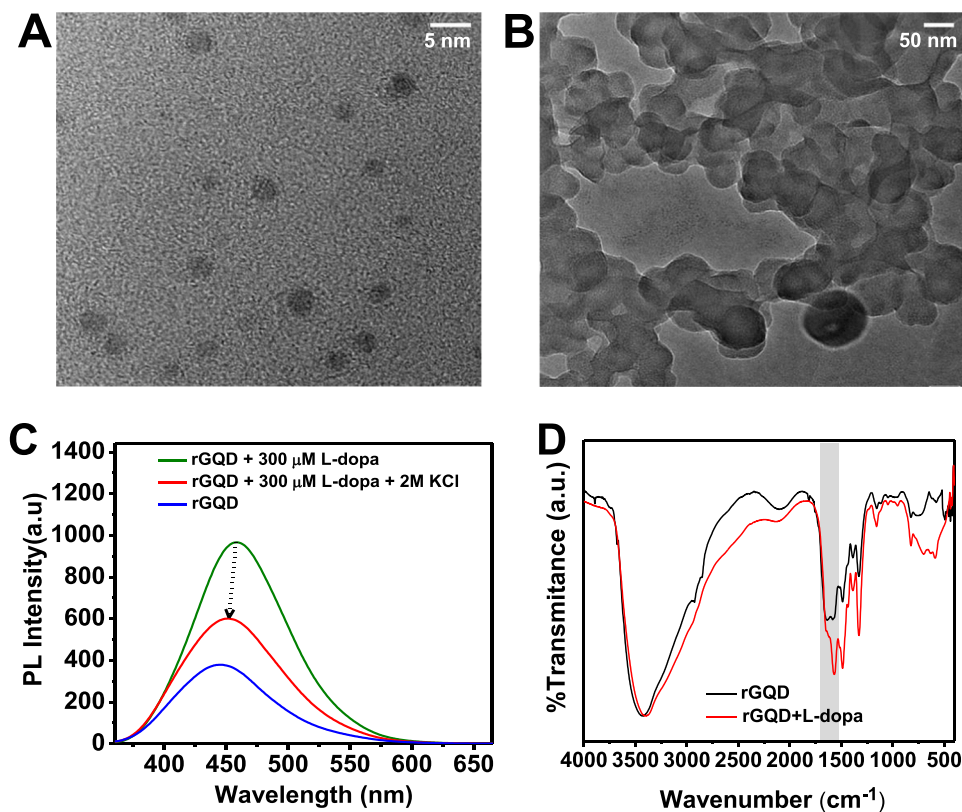


Fig. 3. TEM images of A. rGQD (5 nm), and B. rGQD + L-dopa (50 nm). C. Salt screening effect experiment using fluorescence spectra of rGQD in the presence of L-dopa and 2 M KCl solution. D. FT-IR spectra of rGQD, rGQD + L-dopa.

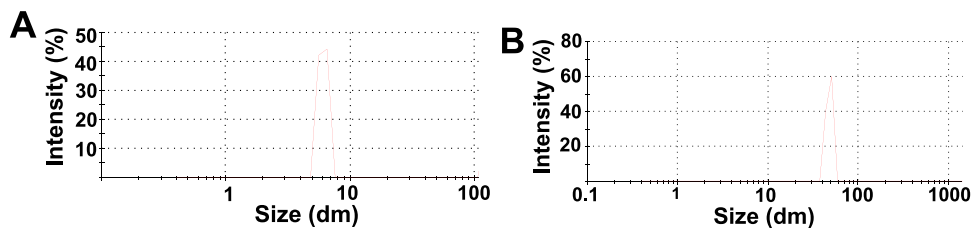


Fig. 4. DLS measurement: particle size distribution plot of A. rGQD, B. rGQD + L-Dopa.

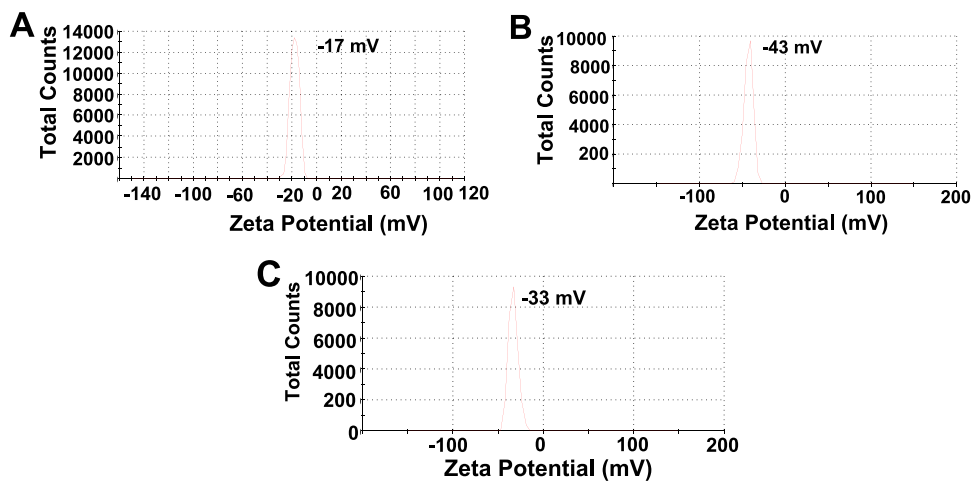


Fig. 5. DLS measurement: Zeta-potential distribution plot of A. L-dopa, B. rGQD, C. rGQD + L-Dopa.

Table 1

Analysis of real sample for L-dopa in human blood plasma sample and recoveries at five concentrations of L-dopa. (n = 3).

Sl No.	L-dopa spiked/(μM)	Found/(μM)	Recovery/%	RSD/%
1	10	10.29	102.9	3.16
2	20	19.49	97.4	2.38
3	30	29.14	97.1	3.65
4	40	39.33	98.3	3.49
5	50	50.37	100.7	2.80

be in the range of 97.1–102.9%. Table 1 with RSD from 2.38% to 3.65% indicating the reliability and sensitivity of the sensor towards the determination of L-dopa in real samples [53].

Earlier we have demonstrated the fluorescence enhancement in AU with varying concentrations of L-dopa. To check the practical applicability in a real urine sample, three (n = 3) measurements have been performed at 70 μM concentration of L-dopa and the results are shown in Table S1. In a similar experiment, Smyth et al., were able to recover 1.87 $\mu\text{g mL}^{-1}$ from urine samples after spiking with 2 $\mu\text{g mL}^{-1}$ of L-dopa [52]. Therefore, from these measurements using human blood plasma and real-urine sample, it can be confirmed that the present system is applicable not only in aqueous media but also in real samples.

3.2.5. Visual detection of L-dopa

For visual detection of L-dopa, we have collected the digital photographs of rGQD solutions under 365 nm UV light irradiation. As evident from Fig. 6A, the rGQD develops bright blue fluorescence after the interaction with L-dopa dissolved in AU. In a different approach, filter paper strips were treated with rGQD and the change in their

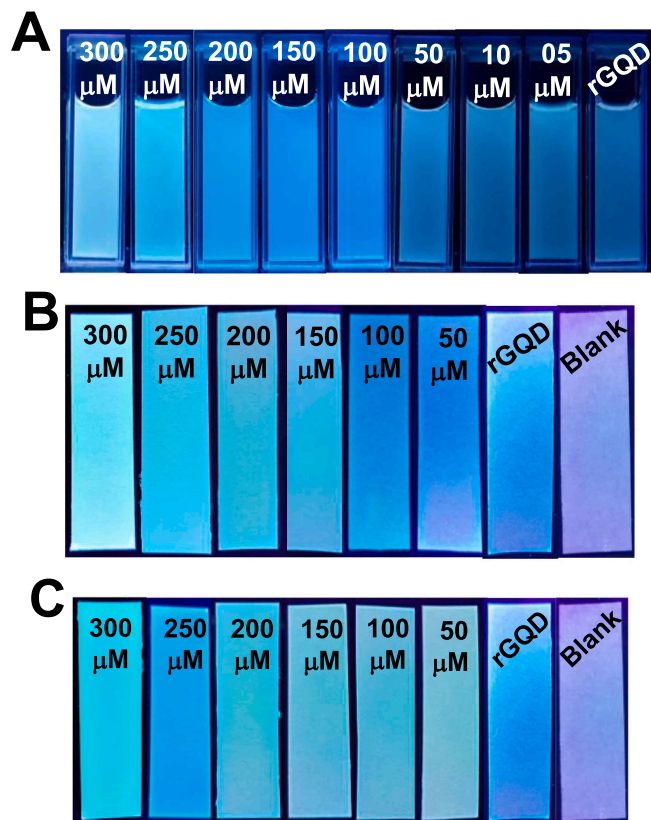


Fig. 6. Digital photographs in UV cabinet (365 nm): A. rGQD and rGQD + L-dopa in AU. Filter paper strips treated with rGQD and varying concentrations of L-dopa in B. Aqueous media, and C. AU.

fluorescence for L-dopa present in aqueous media and AU was observed under UV irradiation (Fig. 6B and C). The results are similar to that of the solution phase as the filter paper strips develop bright blue colours at room temperature. The use of filter paper is one of the most cost-effective methods for the detection of the different analytes. Handling of paper-based sensors is easy and can be stored in ambient conditions [54]. Therefore, this method is effective for the low-cost production of L-dopa sensors from rGQD treated filter papers.

3.2.6. Electrical measurement-based sensing

Before starting the sensing experiment, we checked the air-stability of the sensor by measuring its impedance (Z) with varying relative humidity from 20% to 90%, as presented in Fig. 7A. It was observed that the Z of the devices remain unchanged, which indicates that varying humidity conditions don't alter the electrical properties of the sensor and hence the sensor can be useful for measuring ambient conditions. For the sensing experiments, I-V characteristics and ionic conduction of the sensor were measured before and after the interaction with increasing concentration of L-dopa ranging from 5 to 300 μM . Similar to the fluorescence measurements, the presence of L-dopa significantly alters the electrical properties of PVA + rGQD films, as shown in Fig. 7B. At a maximum of 300 μM of L-dopa, there was a 2.5 order increase in the current density at a maximum applied voltage of 5 V. From the calibration plot (Fig. 7C), the LOD was calculated to be 13.136 μM .

Similarly, the interaction of L-dopa also increases the percent ionic character of the device, which has been observed by measuring the DC current density at the fixed voltage of 0.1 V with respect to time as shown in Fig. 8A. Here, at a constant DC voltage, migration of ions takes place until the sample is fully polarized. Here, the two silver electrodes act as ion blocking electrodes. When the steady-state is achieved, the material shows only electronic conduction [55]. From this plot, the percentage ionic character was calculated by using the following equation, $t_{\text{ion}} = (i_T - i_e)/i_T \times 100$, where i_e and i_T are the residual and total current, respectively. In the present case, PVA and its composite with rGQDs initially show electronic conduction and develop about 89% ionic conduction in the presence of L-dopa. During these electrical measurements, the film retained its structural integrity, which was confirmed under SEM as discussed in the later section. In continuation of Section 2.2, a flexible device architecture was realized to check the potential of this method as wearable biosensors. Similar to the results of I-V measurements of conventional methods, the flexible device also develops one order increase in the current conduction at 200 μM concentration of L-dopa (Fig. 8B).

In practical applications, wearable devices must operate under extreme bending angles and hence we checked the I-V characteristics of the flexible device at 180° and about 90° bending angles. Digital photographs of the device are shown in Fig. 9A at 180° and 90° bending angles. Additionally, in Fig. 9B, the I-V characteristics of the flexible device are also presented for four different cycles and evidently, the device generates similar current conduction in these cycles. The structural integrity of the sensing materials play a vital role in this experiment. Here, the 8% PVA (W/V) provides a strong adhesion with the PET substrate and also creates a transparent and stretchable thin film under the device fabrication conditions. The PVA + rGQD films possess a very smooth surface morphology, and unlike macroporous polymers, no significant surface patterns were observed under SEM. After the treatment with L-dopa, other than the nanometer-sized particles on the surface, there was no notable change in the surface morphology of the film architecture as shown in Fig. S5A–C. This observation was particularly important for developing flexible devices for electrical sensing experiments. Here, it was essential to maintain a structural integrity of the films to ensure similar electrical properties at different bending angles, which is not possible with porous polymer films.

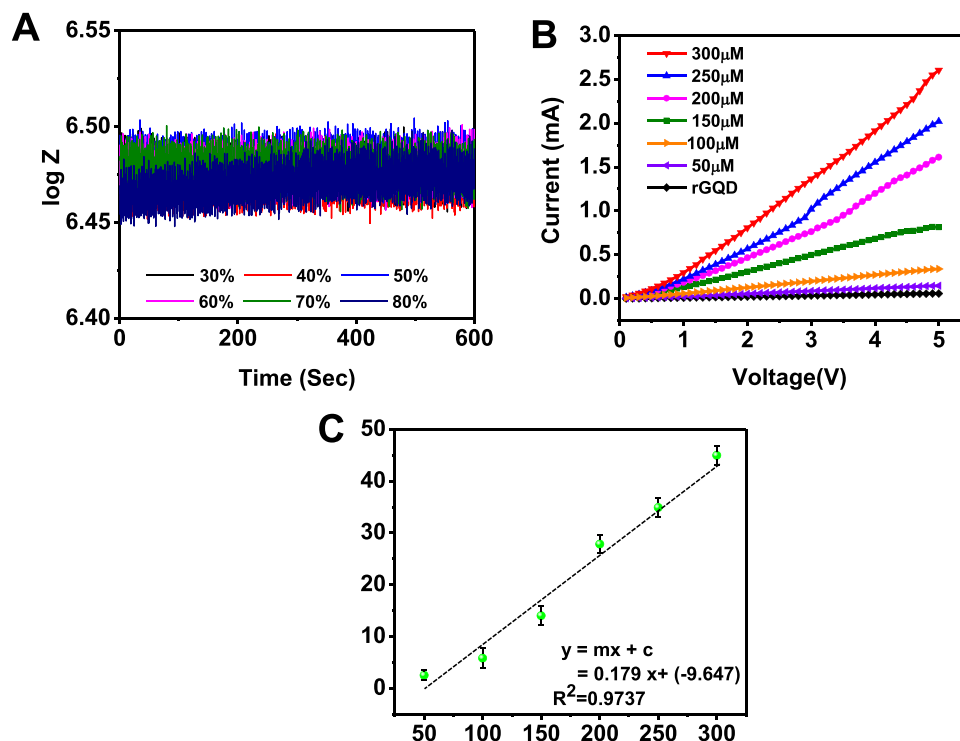


Fig. 7. A. logZ versus Time plot of the rGQD + PVA film at different relative humidity (include) B. I-V characteristics of the rGQD + PVA films with increasing concentration of L-dopa. C. Calibration plot.

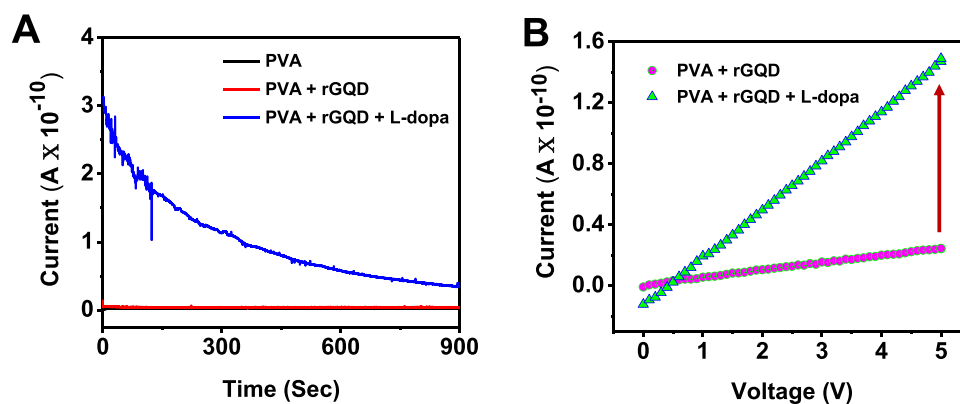


Fig. 8. A. Current versus time plot of PVA, PVA + rGQD, PVA + rGQD + L-dopa. B. I-V characteristics of flexible devices with PVA + rGQD, PVA + rGQD + L-dopa.

4. Comparative study

In literature, there are different methods of L-dopa detection. Herein, a brief comparative study has been conducted based on the limit of detection of the fluorescence measurements as given in Table 2. In comparison to the already reported methods, there are three major aspects that make the present work readily distinguishable and unique compared to the other methods.

Firstly, the present study reports a triple mode detection of L-dopa based on the same starting material viz. fluorescence turn-on, filter paper-based sensing, and electrical and flexible electronic device-based sensing of L-dopa. The quick response of all the three modes toward the analyte with an appreciable limit of detection compared to the reported

sensors.

Secondly, the photophysical methods are applicable in real sample analysis as it shows efficient fluorescence enhancement in human blood plasma, artificial and real artificial urine samples.

Thirdly, the methods do not require sophisticated instrumentation facilities for device fabrication and sensing experiments. The device fabrication is extremely simple and low-cost, ensuring practical applicability of the sensor in resource-limited and urgent requirement situations for developing a biosensor. Additionally, the devices are air-stable and show bending stability which is rare, particularly in the case of electronics.

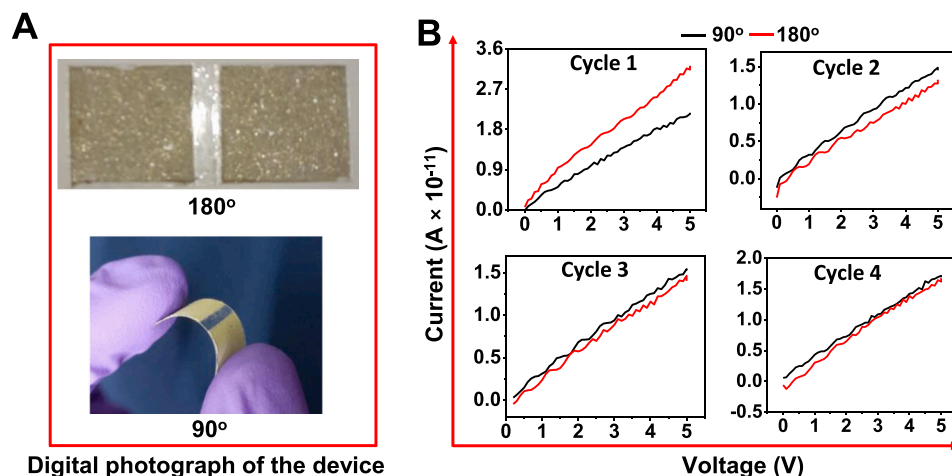


Fig. 9. A. digital photograph of the flexible device. B. *I-V* characteristics of the rGQD + PVA flexible devices at 200 μM concentration of L-dopa.

Table 2

Comparison of the materials, methods, and the limit of detection (LOD) of the reported L-dopa sensors based on fluorescence measurements.

Sl No.	Material	Method	Detection range (μM)	LOD	Reference
1	Polylevodopa Nanoparticles	Fluorescence turn-on	0.3–100	29.0 nM	[23]
2	Zn(II)-terpyridine complexes	Fluorescence turn-off	0–140	3 (μM)	[56]
3	Phenylboronic acid derivative of (Lucifer yellow dye)	Fluorescence quenching	0–5000	5 (μM)	[21]
4	Reduced graphene oxide quantum dots (rGQDs)	Fluorescence turn-on	5–300	1.30 (μM)	This work

5. Conclusion

The present work demonstrated a new approach towards the selective and sensitive detection of L-dopa in aqueous media as well as in artificial urine using rGQD. The rGQD undergoes significant fluorescence turn-on in the presence of L-dopa with a LOD of about 1.307 μM . This fluorescence turn-on is predominantly governed by AIE mechanism which is also supported by different experimental evidences such as TEM, salt screening effect, and DLS. The practical applicability of this method was also investigated by spiking different concentrations of L-dopa in human blood serum and real urine samples. In addition, rGQD treated filter papers develop bright fluorescence in the presence of L-dopa under UV-light irradiation, which is helpful for visual detection of L-dopa in aqueous and artificial urine. Such filter paper-based detection is very easy and helpful in the case of rapid drug sensing applications. On the other hand, electrical measurement-based sensing was carried out by investigating the current-voltage characteristics of the rGQD with PVA based thin films under ambient conditions. This method has a limit of detection of about 13.136 μM . More importantly, electronic devices were fabricated using a facile fabrication technique on a flexible substrate to demonstrate the practical applicability of the method as a wearable biosensor. These devices are air-stable, and their electrical properties do not vary with increasing relative humidity. We have also found that the electrical properties of the sensors remain similar at different bending angles. Using such flexible prototype devices, it would be possible to design wearable L-dopa sensors in the future.

CRediT authorship contribution statement

Kangkan Jyoti Goswami: Conceived the idea of sensing L-dopa using fluorescence measurements, sample preparation, sensing experiments, data analysis, and manuscript preparation. **Bedanta Gogoi:** Conceived the idea of sensing L-dopa using electrical measurements, manuscript preparation, and Supervision. **Neelotpal Sen Sarma:** Supervision and manuscript preparation.

Declaration of Competing Interest

The authors declare no conflicts of interest.

Acknowledgements

KJG and NSS acknowledge DST, Government of India for financial support. BG acknowledge the Department of Science and Technology (DST), Government of India for financial support under INSPIRE faculty scheme (IFA18-CH 313).

Appendix A. Supporting information

Supplementary data associated with this article can be found in the online version at [doi:10.1016/j.snb.2021.130892](https://doi.org/10.1016/j.snb.2021.130892).

References

- [1] A.J. Lees, Unresolved issues relating to the shaking palsy on the celebration of James Parkinson's 250th birthday, *Mov. Disord.: Off. J. Mov. Disord. Soc.* 22 (2007) S327–S334.
- [2] M.C. De Rijk, W. Rocca, D. Anderson, M. Melcon, M. Breteler, D. Maraganore, A population perspective on diagnostic criteria for Parkinson's disease, *Neurology* 48 (1997) 1277–1281.
- [3] J. Dorszewska, M. Prendecki, M. Lianeri, W. Kozubski, Molecular effects of L-dopa therapy in Parkinson's disease, *Curr. Genom.* 15 (2014) 11–17.
- [4] G. Rao, L. Fisch, S. Srinivasan, F. D'Amico, T. Okada, C. Eaton, C. Robbins, Does this patient have Parkinson disease? *JAMA* 289 (2003) 347–353.
- [5] R. Balestrino, A. Schapira, Parkinson disease, *Eur. J. Neurol.* 27 (2020) 27–42.
- [6] B.S. Connolly, A.E. Lang, Pharmacological treatment of Parkinson disease: a review, *JAMA* 311 (2014) 1670–1683.
- [7] W. Poewe, K. Seppi, C.M. Tanner, G.M. Halliday, P. Brundin, J. Volkmann, A. E. Schrag, A.E. Lang, Parkinson disease, *Nat. Rev. Dis. Prim.* 3 (2017) 1–21.
- [8] N.B. Mercuri, G. Bernardi, The 'magic' of L-dopa: why is it the gold standard Parkinson's disease therapy? *Trends Pharmacol. Sci.* 26 (2005) 341–344.
- [9] S. Sandeep, A.S. Santhosh, N.K. Swamy, G.S. Suresh, J.S. Melo, K.S. Nithin, Electrochemical detection of L-dopa using crude Polyphenol oxidase enzyme immobilized on electrochemically reduced RGO-Ag nanocomposite modified graphite electrode, *Mater. Sci. Eng.: B* 232 (2018) 15–21.
- [10] N.F. Atta, A. Galal, E.H. El-Ads, A.E. Galal, Efficient electrochemical sensor based on gold nanoclusters/carbon ionic liquid crystal for sensitive determination of neurotransmitters and anti-Parkinson drugs, *Adv. Pharm. Bull.* 10 (2020) 46–55.

- [11] K.Y. Goud, C. Moonla, R.K. Mishra, C. Yu, R. Narayan, I. Litvan, J. Wang, Wearable electrochemical microneedle sensor for continuous monitoring of levodopa: toward Parkinson management, *ACS Sens.* 4 (2019) 2196–2204.
- [12] A.M. Lozano, A.E. Lang, W.D. Hutchison, J.O. Dostrovsky, New developments in understanding the etiology of Parkinson's disease and in its treatment, *Curr. Opin. Neurobiol.* 8 (1998) 783–790.
- [13] B. Rezaei, L. Shams-Ghahfarokhi, E. Havakeshian, A.A. Ensaifi, An electrochemical biosensor based on nanoporous stainless steel modified by gold and palladium nanoparticles for simultaneous determination of levodopa and uric acid, *Talanta* 158 (2016) 42–50.
- [14] B. Thanvi, T. Lo, Long term motor complications of levodopa: clinical features, mechanisms, and management strategies, *Postgrad. Med. J.* 80 (2004) 452–458.
- [15] T. Terse-Thakoor, S. Badhulika, A. Mulchandani, Graphene based biosensors for healthcare, *J. Mater. Res.* 32 (2017) 2905–2929.
- [16] S. Szenerits, R. Boukherroub, Graphene-based biosensors, *Interface Focus* 8 (2018), 20160132.
- [17] L. Soleymani, F. Li, Mechanistic challenges and advantages of biosensor miniaturization into the nanoscale, *ACS Sens.* 2 (2017) 458–467.
- [18] M. Mathew, S. Radhakrishnan, A. Vaidyanathan, B. Chakraborty, C.S. Rout, Flexible and wearable electrochemical biosensors based on two-dimensional materials: recent developments, *Anal. Bioanal. Chem.* (2020) 1–36.
- [19] K. Yang, H. Peretz-Soroka, Y. Liu, F. Lin, Novel developments in mobile sensing based on the integration of microfluidic devices and smartphones, *Lab a Chip* 16 (2016) 943–958.
- [20] L. Wang, D. Su, S.N. Berry, J. Lee, Y.-T. Chang, A new approach for turn-on fluorescence sensing of l-DOPA, *Chem. Commun.* 53 (2017) 12465–12468.
- [21] A. Coskun, E.U. Akkaya, Three-point recognition and selective fluorescence sensing of l-DOPA, *Org. Lett.* 6 (2004) 3107–3109.
- [22] X.-X. Chen, X. Wu, P. Zhang, M. Zhang, B.-N. Song, Y.-J. Huang, Z. Li, Y.B. Jiang, Multicomponent covalent dye assembly for tight binding and sensitive sensing of l-DOPA, *Chem. Commun.* 51 (2015) 13630–13633.
- [23] M.R. Hormozi-Nezhad, A. Moslehpour, A. Bigdeli, Simple and rapid detection of l-dopa based on in situ formation of polylevodopa nanoparticles, *Sens. Actuators B: Chem.* 243 (2017) 715–720.
- [24] Y.-C. Chou, C.-I. Shih, C.-C. Chiang, C.-H. Hsu, Y.-C. Yeh, Reagent-free DOPA-dioxygenase colorimetric biosensor for selective detection of l-DOPA, *Sens. Actuators B: Chem.* 297 (2019), 126717.
- [25] C. Hansson, G. Agrup, H. Rorsman, A.-M. Rosengren, E. Rosengren, L.-E. Edholm, Analysis of cysteinyl-dopa, dopa, dopamine, noradrenaline and adrenaline in serum and urine using high-performance liquid chromatography and electrochemical detection, *J. Chromatogr. B: Biomed. Sci. Appl.* 162 (1979) 7–22.
- [26] B.A. Hasan, K.D. Khalaf, M. De La Guardia, Flow analysis-spectrophotometric determination of l-dopa in pharmaceutical formulations by reaction with p-aminophenol, *Talanta* 42 (1995) 627–633.
- [27] J. Luo, Z. Xie, J.W. Lam, L. Cheng, H. Chen, C. Qiu, H.S. Kwok, X. Zhan, Y. Liu, D. Zhu, B.Z. Tang, Aggregation-induced emission of 1-methyl-1, 2, 3, 4, 5-pentaphenylsilole, *Chem. Commun.* (2001) 1740–1741.
- [28] N.B. Shustova, B.D. McCarthy, M. Dinca, Turn-on fluorescence in tetraphenylethylene-based metal-organic frameworks: an alternative to aggregation-induced emission, *J. Am. Chem. Soc.* 133 (2011) 20126–20129.
- [29] N.B. Shustova, T.-C. Ong, A.F. Cozzolino, V.K. Michaelis, R.G. Griffin, M. Dinca, Phenyl ring dynamics in a tetraphenylethylene-bridged metal-organic framework: implications for the mechanism of aggregation-induced emission, *J. Am. Chem. Soc.* 134 (2012) 15061–15070.
- [30] B. He, S. Ye, Y. Guo, B. Chen, X. Xu, H. Qiu, Z. Zhao, Aggregation-enhanced emission and efficient electroluminescence of conjugated polymers containing tetraphenylethylene units, *Sci. China Chem.* 56 (2013) 1221–1227.
- [31] Y. Chen, J.W. Lam, R.T. Kwok, B. Liu, B.Z. Tang, Aggregation-induced emission: fundamental understanding and future developments, *Mater. Horiz.* 6 (2019) 428–433.
- [32] R. Guo, T. Li, S. Shi, Aggregation-induced emission enhancement of carbon quantum dots and applications in light emitting devices, *J. Mater. Chem. C* 7 (2019) 5148–5154.
- [33] J.R. Adsetts, S. Hoesterey, C. Gao, D.A. Love, Z. Ding, Electrochemiluminescence and photoluminescence of carbon quantum dots controlled by aggregation-induced emission, aggregation-caused quenching, and interfacial reactions, *Langmuir* 36 (2020) 14432–14442.
- [34] D. Ozyurt, S. Shafiqat, T.T. Pakkanen, R.K. Hocking, A. Mouritz, B. Fox, Aggregation induced emission transformation of liquid and solid-state N-doped graphene quantum dots, *Carbon* 175 (2021) 576–584.
- [35] R.V. Nair, R.T. Thomas, V. Sankar, H. Muhammad, M. Dong, S. Pillai, Rapid, acid-free synthesis of high-quality graphene quantum dots for aggregation induced sensing of metal ions and bioimaging, *ACS Omega* 2 (2017) 8051–8061.
- [36] J. Chang, H. Li, T. Hou, F. Li, based fluorescent sensor for rapid naked-eye detection of acetylcholinesterase activity and organophosphorus pesticides with high sensitivity and selectivity, *Biosens. Bioelectron.* 86 (2016) 971–977.
- [37] N. Zaaba, K. Foo, U. Hashim, S. Tan, W.-W. Liu, C. Voon, Synthesis of graphene oxide using modified hummers method: solvent influence, *Procedia Eng.* 184 (2017) 469–477.
- [38] N.H. Kim, T. Kuila, J.H. Lee, Simultaneous reduction, functionalization and stitching of graphene oxide with ethylenediamine for composites application, *J. Mater. Chem. A* 1 (2013) 1349–1358.
- [39] S.B. Maddinedi, B.K. Mandal, R. Vankayala, P. Kalluru, S.R. Pamanji, Bioinspired reduced graphene oxide nanosheets using *Terminalia chebula* seeds extract, *Spectrochim. Acta Part A: Mol. Biomol. Spectrosc.* 145 (2015) 117–124.
- [40] J.U. Lee, W. Lee, J.W. Yi, S.S. Yoon, S.B. Lee, B.M. Jung, B.S. Kim, J.H. Byun, Preparation of highly stacked graphene papers via site-selective functionalization of graphene oxide, *J. Mater. Chem. A* 1 (2013) 12893–12899.
- [41] B. Xue, J. Zhu, N. Liu, Y. Li, Facile functionalization of graphene oxide with ethylenediamine as a solid base catalyst for Knoevenagel condensation reaction, *Catal. Commun.* 64 (2015) 105–109.
- [42] F. Zhou, H.N. Tien, Q. Dong, W.L. Xu, H. Li, S. Li, M. Yu, Ultrathin, ethylenediamine-functionalized graphene oxide membranes on hollow fibers for CO₂ capture, *J. Membr. Sci.* 573 (2019) 184–191.
- [43] F. Samadaei, M. Salami-Kalajahi, H. Roghani-Mamaqani, M. Banaei, A structural study on ethylenediamine-and poly (amidoamine)-functionalized graphene oxide: simultaneous reduction, functionalization, and formation of 3D structure, *RSC Adv.* 5 (2015) 71835–71843.
- [44] S. Alex, H.L. Thanh, D. Vocelle, Studies of the effect of hydrogen bonding on the absorption and fluorescence spectra of all-trans-retinal at room temperature, *Can. J. Chem.* 70 (1992) 880–887.
- [45] P. Yadav, A.K. Singh, C. Upadhyay, V.P. Singh, Photoluminescence behaviour of a stimuli responsive Schiff base: aggregation induced emission and piezochromism, *Dyes Pigments* 160 (2019) 731–739.
- [46] B. Gogoi, N.Sen Sarma, Curcumin-cysteine and curcumin-tryptophan conjugate as fluorescence turn on sensors for picric acid in aqueous media, *ACS Appl. Mater. Interfaces* 7 (2015) 11195–11202.
- [47] B. Gogoi, N. Paul, D. Chowdhury, N.S. Sarma, Instant detection of picric acid vapour by developing layer by layer polymer detectors and an electronic prototype, *J. Mater. Chem. C* 3 (2015) 11081–11089.
- [48] V. Uskoković, Z. Castiglione, P. Cubas, L. Zhu, W. Li, S. Habelitz, Zeta-potential and particle size analysis of human amelogelins, *J. Dent. Res.* 89 (2010) 149–153.
- [49] S. Chakravarty, B. Gogoi, B.B. Mandal, N. Bhardwaj, N.S. Sarma, Silk fibroin as a platform for dual sensing of vitamin B12 using photoluminescence and electrical techniques, *Biosens. Bioelectron.* 112 (2018) 18–22.
- [50] P. Dutta, D. Saikia, N.C. Adhikary, N.S. Sarma, Macromolecular systems with MSA-Capped CdTe and CdTe/ZnS Core/Shell quantum dots as superselective and ultrasensitive optical sensors for picric acid explosive, *ACS Appl. Mater. Interfaces* 7 (2015) 24778–24790.
- [51] D.Q. Lin, P.J. Brixius, J.J. Hubbuch, J. Thömmes, M.R. Kula, Biomass/adsorbent electrostatic interactions in expanded bed adsorption: a zeta potential study, *Biotechnol. Bioeng.* 83 (2003) 149–157.
- [52] K.A. Sagar, M.R. Smyth, Simultaneous determination of levodopa, carbidopa and their metabolites in human plasma and urine samples using LC-EC, *J. Pharm. Biomed. Anal.* 22 (2000) 613–624.
- [53] S. Geng, S.M. Lin, S.G. Liu, N.B. Li, H.Q. Luo, A new fluorescent sensor for detecting p-nitrophenol based on β -cyclodextrin-capped ZnO quantum dots, *RSC Adv.* 6 (2016) 86061–86067.
- [54] B. Kalita, B. Gogoi, N.S. Sarma, Cholesterol-amino acid conjugates treated filter paper-based photoluminescence indicator for nitroaromatic chemicals, *Mater. Res. Bull.* 115 (2019) 211–218.
- [55] B. Gogoi, P. Dutta, N. Paul, N.N. Dass, N.S. Sarma, Polycurcumin acrylate and polycurcumin methacrylate: novel bio-based polymers for explosive chemical sensor, *Sens. Actuators B: Chem.* 181 (2013) 144–152.
- [56] I.J. Bazany-Rodríguez, M.K. Salomón-Flores, A.O. Viviano-Posadas, M.A. García-Lleno, J. Barroso-Flores, D. Martínez-Otero, A. Dorazco-González, Chemosensing of neurotransmitters with selectivity and naked eye detection of l-DOPA based on fluorescent Zn (ii)-terpyridine bearing boronic acid complexes, *Dalton Trans.* 50 (2021) 4255–4269.

Kangkan Jyoti Goswami is a Ph.D. student in Advance Material Laboratory, Physical Sciences Division, Institute of Advanced Study in Science and Technology (IASST). He has completed his M.Sc. degree from Assam University, Department of chemistry, Silchar in 2016 and joined IASST on 31st January, 2020 under the supervision of Prof. Neelotpal Sen Sarma. His field of interest is on biopolymer based chemical sensors.

Dr. Bedanta Gogoi completed his Ph.D. in the year 2016 from the Institute of Advanced Study in Science and Technology (IASST) under the supervision of Prof. Neelotpal Sen Sarma, and joined as INSPIRE faculty at the Department of Chemistry, Gauhati University in the year 2019. He worked as a visiting researcher at The Petroleum Institute, Abu Dhabi in 2014, and also worked as a postdoctoral researcher at the Weizmann Institute of Science, Israel from 2016 to 2019. His research interest are optoelectronics, polymer chemistry, nanochemistry, self-assembly, and sensors. So far he has 15 research articles in international journals, two book chapters, and one patent application to his credit.

Prof. Neelotpal Sen Sarma did his Ph.D. in the year 2001 and joined Institute of Advanced Study in Science and Technology (IASST) in the year 2002. He did his M.Sc. from Dibrugarh University, M.Tech. from Indian Institute of Science (IISc), Bangalore and Pet. Tech. diploma from Dibrugarh University. His research interest is on Sensors, LC polymers, Solid state ionics, Hydrogels, Nanocomposites, Biosorbents, etc. and he so-far published 97 research papers in National and International Journals, applied for three patents and received two patents on solid state ionics and LC polymer.